Tracking spatial modes in nearly hemispherical microcavities

R. C. Pennington,[1,*] G. D'Alessandro,[2] J. J. Baumberg,[1] and M. Kaczmarek[1]

[1]School of Physics and Astronomy, University of Southampton, Highfield, Southampton SO17 1BJ, England
[2]School of Mathematics, University of Southampton Highfield, Southampton SO17 1BJ, England
*Corresponding author: rpennington@phys.soton.ac.uk

Received July 23, 2007; revised September 20, 2007; accepted September 20, 2007;
posted September 25, 2007 (Doc. ID 85031); published October 22, 2007

We measure experimentally the spatial intensity profiles and resonant frequencies of the transverse modes of nearly hemispherical microcavities with cavity length and mirror curvatures below 10 μm. These resonators possess axially symmetric Gauss–Laguerre-like modes, but do not display the frequency degeneracies typical of large-scale optical cavities. It is possible to interpret these results using a paraxial model of cavity propagation that includes nonparabolic optical elements. © 2007 Optical Society of America

OCIS codes: 140.4780, 230.3990, 220.4000, 260.3910.

Microcavities are one of the most useful micro-optical components because of the sharp resonances and small volume of their modes. They can be applied in many novel devices such as ultralow-threshold lasers and miniaturized nonlinear optical components, enhanced emitters, tunable microfilters, enhanced sensors, and resonant light–matter modulators [1–3]. Until now, the main microcavity structures studied have been planar, pillar, photonic crystal, and whispering gallery designs. Embedded quantum dots or quantum wells inside pillar microcavities give enhanced emission and nonlinear optical response [4–6]. On the other hand, the design and fabrication of empty microcavities, which can be subsequently filled with active (in)organic materials is difficult. For example, planar microcavities are easy to fill, but confine photons in only one direction [2]. We have recently built cavities with spherical micromirrors that overcome this problem: the planar structure of the device allows for easy filling, while the spherical micromirror strongly confines the modes. Here we report the experimental and theoretical characterization of their transverse mode spectrum. This shows some unexpected features: the modes are Gauss–Laguerre (GL)-like and axially symmetric, but the frequency degeneracies typical of GL modes, with different radial indices, are lifted.

Our planar-spherical microcavities [Fig. 1(a)] are formed by assembling a template of latex spheres and electrochemically growing gold around them. The spheres are dissolved away, leaving hemispherical dishes of controllable height, which are combined with gold-coated planar top mirrors to form a microcavity (for fabrication details see [7]). These structures have the advantage of being very robust and easy to fabricate. They are also widely tunable by varying the cavity length, L, and the radius of curvature, R, of the hemispherical dish. Such empty cavities can be filled with liquid crystals, dyes, or quantum dots. Our previous work has shown that this type of geometry is important for controlling defects in incorporated liquid crystals and gives significantly improved optical switching times [8]. Similar microcavities have been subsequently suggested for modifying emission from single semiconductor quantum dots [9].

By confining the light in the plane as well as vertically, the cavity modes become discrete and split into longitudinal and transverse modes [Fig. 1(b)]. While paraxial theory is sufficient to describe such cavities on scale lengths much larger than the wavelength of light, at present there are no adequate theories for these micrometer scale structures. Our previous work using hemispherical dishes and gold-tipped optical fibers showed that both transverse and longitudinal modes can be seen [7], but did not resolve the spatiospectral mode structure. Here we evanescently couple incoherent white light from a blackbody source through the thin gold at the base of the dish mirror. The transmission spectra are recorded on a confocally arranged fiber-coupled monochromator and cooled CCD. Spectra are measured as the microcavity is laterally scanned using piezoelectric stages, allowing us to build up a map of the emerging spectral modes at each position across the microcavity.

The experimentally measured transverse cavity spectrum (Fig. 2) is superficially similar to the spectrum of a paraxial cavity with parabolic optical elements [10]. In such cavities the modes can be written as $A_{npq}=G_{pq}(r,\phi,z)e^{i\pi nz}$, where z is the coordinate along the cavity axis, scaled to cavity length L, while r and ϕ are polar coordinates in the transverse plane. The radial distances are in units of $\sqrt{L\lambda}/\pi$, where λ is the optical wavelength. The three indices n, p, and q

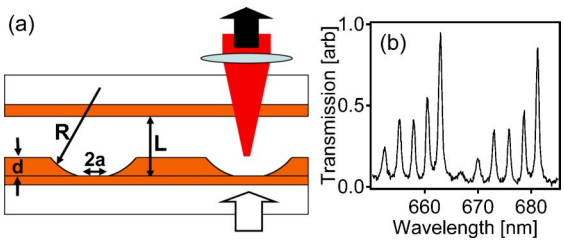

Fig. 1. (Color online) (a) Geometry of microcavity (R, radius of curvature; L, cavity length; a, radius of flat bottom; d, dish thickness) and experimental setup, with (b) typical transmission spectrum spanning two longitudinal mode families.

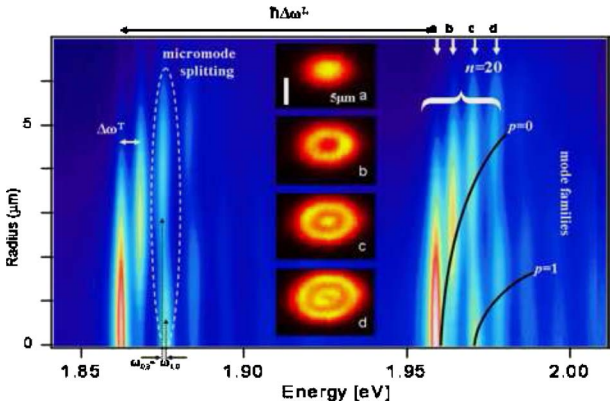

Fig. 2. (Color online) Radial intensity profiles of the transmitted light as a function of energy, showing families of p modes for a cavity $L=6.5$ μm, $R=10$ μm. Inset: spatial intensity distributions at energies shown by arrows labeled a–d.

are integers, with the longitudinal mode index $n>0$. The function $G_{pq}(r,\phi,z)$ is the transverse mode profile and, in the plane of the minimum beam waist, is given by

$$G_{pq}(r,\phi,z)=\frac{(\sqrt{2}r)^{|q|}}{\sqrt{2\pi}w_0}L_p^{|q|}\left(\sqrt{2}\frac{r^2}{w_0^2}\right)e^{-r^2/w_0^2+iq\phi}, \qquad (1)$$

where w_0 is the minimum beam waist and $L_p^{|q|}(x)$ is the generalized Laguerre polynomial of order p and parameter $|q|$ [11]. From this formula we see that the radial index $p>0$ is equal to the number of zeros of the field in the radial direction, while the azimuthal index q is the phase winding number of the mode. The frequency of a mode (n,p,q) in units of the cavity round-trip frequency $(\Delta\omega^L=\pi c/L)$ is given by

$$\tilde{\omega}_{npq}=n-\theta_{\mathrm{Au}}+(2p+q+1)\Delta\tilde{\omega}^T, \qquad (2)$$

where the expected transverse mode spacing $\Delta\tilde{\omega}^T=\arcsin(\sqrt{L/R})/\pi$, and θ_{Au} is the phase shift on reflection from the Au film [12]. In this conventional limit, transverse modes are equispaced and modes with the same value of $2p+|q|$ are frequency degenerate. If the cavity is not axially symmetric, the mode structure remains unaltered, but one has to use Cartesian coordinates in Eq. (1) and express the function G_{pq} as an appropriate product of Hermite polynomials and Gaussian functions (Gauss–Hermite modes).

Here we show that, while Eqs. (1) and (2) capture the qualitative features of the spectrum, there are significant differences to be explained. Experimental data (Fig. 2) on a typical cavity with $R=10$ μm, $L=6.5$ μm clearly demonstrates the different families of modes observed. Similar data is seen on many different microcavities, and for different cavity lengths. In all cases *circularly* symmetric GL modes are seen (inset shows detailed spatial maps of modes for different energies, indicated by arrows), rather than the Hermite–Gauss modes observed in *all* macroscale cavities. Invariably even slight astigmatism present in every large-scale cavity is enough to split the modes into orthogonal linear families of TE_{mn} modes, but this effect is completely suppressed in these micrometer-scale cavities. For each longitudinal index n, two families of GL modes are seen, each with increasing azimuthal mode index, $q=0,1,2,3,4$, which form annular modes of increasing diameter. Surprisingly the $q>0$ modes are visible despite the fact that they are forbidden in this symmetrical coupling geometry (as the overlap integral between pump and mode is zero). We believe that this symmetry breaking is caused either by roughness around the hole rim or by the fact that the illuminating beam, even though it is of uniform intensity, may not be spatially coherent across the hole of radius a at the vertex of the spherical mirror (see Fig. 1). The radial peak intensity and radial width match the modes of the model within 81%–98% of the fundamental mode. Finally, careful analysis of the spectra (Fig. 2, $n=20$ family) shows that the mode $(p,q)=(1,0)$ has a slightly different frequency from the modes $(p,q)=(0,\pm2)$, contrary to the prediction of Eq. (2).

The mode structure of the microcavities can be determined analytically by solving the full Maxwell's equations with appropriate metal boundary conditions at the gold surfaces and perfectly matched layers in the transverse plane [13]. However, studies of pattern formation in VCSEL [14], of mode spectra in microdisk cavities [15], and of ray dynamics in parabolic cavities [16] indicate that approximations normally used for macroscopic cavities are fairly accurate also in cavities only a few wavelengths in size. The good qualitative agreement between the spectrum of a paraxial cavity with parabolic mirror and the experimental spectra and profiles suggests that the paraxial theory is the correct framework to work in but that we need to include nonparabolic optical elements. This approach is also validated by close inspection of the cavity dish mirrors, which besides being spherical also have a flat circular central facet of radius a to allow light to tunnel into the cavity (Fig. 1). The size of this flat facet can be sensitively controlled through the electrochemical growth conditions. Hence a more accurate model incorporating realistic mirror profiles is required.

We compute the cavity modes using the property that they are the eigenmodes of the cavity propagator $\mathcal{P}_c$. The corresponding eigenvalues give the loss and phase shift per round trip. Formally the cavity propagator is written as the decomposition $\mathcal{P}_c=\mathcal{P}_f\circ\mathcal{M}(r)\circ\mathcal{P}_f$, where $\mathcal{P}_f$ is the free space propagation between the flat and the curved mirror, $\mathcal{M}(r)$ is a multiplicative operator that represents the effect of the curved mirror on the field profile, and the symbol $\circ$ indicates the concatenation of these operators [17]. We use this equation to represent $\mathcal{P}_c$ as a square matrix on a set of GL functions: this makes it straightforward to find its eigenvalues and eigenvectors.

To compare theory and experiment, we extract the "transverse micromode splitting" of the azimuthal modes q and $q+1$, $\Delta\tilde{\omega}_q^T=\tilde{\omega}_{q+1}-\tilde{\omega}_q$. Experimentally this splitting increases almost linearly with index q [Fig. 3(a)], reflecting the increasing mode radius, which thus sees more nonparabolic parts of the mirror. We find this behavior is highly sensitive to the

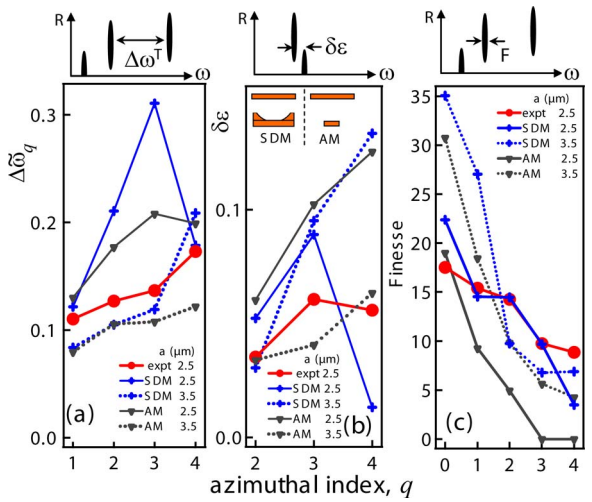

Fig. 3. (Color online) Experimental (red circles) and theoretical: dish model (blue crosses), aperture model (black triangles). (a) Transverse micromode splitting, $\Delta\tilde{\omega}_q^T$; (b) degeneracy lifting, $\delta\epsilon_q$; (c) finesse. $L=9.7$ μm, $R=10$ μm, $p=0$, and experimental flat radius $a=2.5$ μm, with model a as indicated.

size of the flat vertex due to induced coupling with higher-order modes. Deviations of theory from the experiment can be explained by the uncertainty of the precise geometric shape and roughness. Note that the parabolic paraxial approximation gives $\Delta\tilde{\omega}^T=0.6$, much larger than seen experimentally, implying an effective cavity radius of curvature over ten times larger than the physical R.

We also extract the "degenerate lifting," $\delta\epsilon_q=\tilde{\omega}_{p+1,q-2}-\tilde{\omega}_{p,q}$, which should be zero but is split by the nonparabolicity and the micrometer scale of the cavity. We find for both the model and experiment that $\delta\epsilon$ increases with increasing azimuthal mode index [Fig. 3(b)], because the mode experiences more of the nonparabolic edges of the mirror. More puzzling is the order of the modes: $(p,q)=(1,0)$ modes have higher energy than (0,2) modes despite their closer proximity to the mirror center. However the model reproduces this modes' order, arising from the flat facet at the bottom of the spherical micromirror. In addition the model shows that in λ-scale cavities the degeneracy between modes is lifted because the mirror, while circularly symmetric, is not parabolic. In large-scale cavities the reverse is true. Hence here circularly symmetric modes are seen rather than the TE_{mn} splitting.

While a parabolic cavity has equally spaced transverse micromode splitting and no degenerate lifting, we find that the flat bottom can potentially account for the spectral perturbations. We also show the results from a model including just the apertured flat mirror (without curved dish sides), which is known as an unstable resonator on macrosize scales [11]. Its mode spectrum has not been reported so far in the microdomain investigated here. The simple aperture model predicts reduced finesse from incomplete confinement of the transverse mode on the mirror that is not well supported by the data [Fig. 3(c)]. Hence we find that a spherical mirror with flat facet is needed to model these microcavities, though clear differences still exist possibly due to deviations from the spherical profile.

To conclude we measured and modeled the intensity profiles and frequencies of microcavity transverse modes, in the first deviations from the simple paraxial parabolic approximation. Astigmatism has less effect than in cavities of macroscopic scales, giving axially symmetric Gauss–Laguerre modes. Nonparabolicity introduces new effects including induced and unexpected frequency splittings. Understanding the mode structure of microcavities is crucial for exploiting them in applications, as mode mixing drastically changes the mode structure. Such a tie-up between experiments on realizable microcavities and theory presented here can aid in developing and understanding microcavities at the wavelength-scale limit.

References

1. K. J. Vahala, Nature **424**, 839 (2003).
2. F. De Martini, G. Innocenti, G. R. Jacobovitz, and P. Mataloni, Phys. Rev. Lett. **59**, 2955 (1987).
3. M. Trupke, E. A. Hinds, S. Eriksson, E. A. Curtis, Z. Moktadir, E. Kukharenka, and M. Kraft, Appl. Phys. Lett. **87**, 211106 (2005).
4. H. M. Gibbs, G. Khitrova, F. Jahnke, M. Kira, and S. W. Koch, Rev. Mod. Phys. **71**, 1591 (1999).
5. H. Saito, K. Nishi, I. Ogura, S. Sugou, and Y. Sugimoto, Appl. Phys. Lett. **69**, 3140 (1996).
6. M. Benyoucef, S. M. Ulrich, P. Michler, J. Wiersig, F. Jahnke, and A. Forchel, J. Appl. Phys. **97**, 023101 (2005).
7. G. V. Prakash, L. Besombes, T. Kelf, Jeremy J. Baumberg, P. N. Bartlett, and M. E. Abdelsalam, Opt. Lett. **29**, 1500 (2004).
8. G. V. Prakash, M. Kaczmarek, A. Dyadyusha, J. J. Baumberg, and G. D'Alessandro, Opt. Express **13**, 2201 (2005).
9. G. Cui, J. M. Hannigan, R. Loeckenhoff, F. M. Matinaga, M. G. Raymer, S. Bhongale, M. Holland, S. Mosor, S. Chatterjee, H. M. Gibbs, and G. Khitrova, Opt. Express **14**, 2289 (2006).
10. A. Siegman, *Lasers* (University Science Books, 1986).
11. M. Abramowitz and I. A. Stegun, *Handbook of Mathematical Functions*, 9th ed. (Dover, 1964).
12. L. A. Lugiato, G. L. Oppo, J. R. Tredicce, L. M. Narducci, and M. A. Pernigo, J. Opt. Soc. Am. B **7**, 1019 (1990).
13. D. H. Foster and J. U. Nockel, Opt. Commun. **234**, 351 (2004).
14. T. Ackemann, S. Barland, J. R. Tredicce, M. Cara, S. Balle, R. Jager, M. Grabherr, M. Miller, and K. J. Ebeling, Opt. Lett. **25**, 814 (2000).
15. R. P. Wang and M.-M. Dumitrescu, Opt. Lett. **81**, 3391 (1997).
16. J. U. Nockel, G. Bourdon, E. Le Ru, R. Adams, I. Robert, J.-M. Moison, and I. Abram, Phys. Rev. E **62**, 8677 (2000).
17. A. G. Fox and T. Li, Bell Syst. Tech. J. **40**, 453 (1961).